Nuclear Instruments and Methods in Physics Research A262 (1987) 229–242
North-Holland, Amsterdam

PERFORMANCE OF A COMPENSATING LEAD–SCINTILLATOR HADRONIC CALORIMETER

E. BERNARDI [1], G. DREWS [1], M.A. GARCIA [2], R. KLANNER [1], U. KÖTZ [1], G. LEVMAN [3], M. LOMPERSKI [4], D. LÜKE [1], E. ROS [2], F. SELONKE [1], H. TIECKE [5], M. TSIROU [4] and W. VOGEL [6]

[1] *DESY, Hamburg, FRG*
[2] *Univ. Autónoma de Madrid, Spain* *
[3] *Univ. of Toronto, Canada* **
[4] *Univ. of Wisconsin, USA* +
[5] *NIKHEF-H, Amsterdam, The Netherlands*
[6] *Univ. of Hamburg, I. Inst., FRG* ++

Received 29 June 1987

We have built a sandwich calorimeter consisting of 10 mm thick lead plates and 2.5 mm thick scintillator sheets. The thickness ratio between lead and scintillator was optimized to achieve a good energy resolution for hadrons. We have exposed this calorimeter to electrons, hadrons and muons in the energy range between 3 and 75 GeV, obtaining an average energy resolution of $23\%/\sqrt{E}$ for electrons and $44\%/\sqrt{E}$ for hadrons. For energies above 10 GeV and after leakage corrections, the ratio of electron response to hadron response is 1.05.

1. Introduction

The important role to be played by hadronic calorimeters in experiments at high energy accelerators has initiated systematic theoretical and experimental studies to improve their performance.

According to our present knowledge [1–5], the energy resolution of hadronic sampling calorimeters has contributions from sampling fluctuations, which get reduced if the sampling frequency is increased, and contributions due to the strong fluctuations between the different components of hadronic showers (i.e. electromagnetic, ionisation, low energy neutrons, nuclear binding energy, etc.). Whereas the contribution of sampling fluctuations improves with incoming energy E like $1/\sqrt{E}$, part of the fluctuation between different components of the shower produces a constant term which finally dominates at high energy. This constant term can be minimized if the calorimeter is compensating, where compensating means $e/h = 1$, e and h being the fraction of incoming energy detected in the active material of the calorimeter for electrons and hadrons respectively.

* Supported by CAICYT.
** Supported by NSERC.
+ Supported by DOE.
++ Supported by BMFT.

Up to now a ratio e/h close to 1 has been achieved only in sampling calorimeters using depleted uranium as absorber and plastic scintillator as detector [2]. For these calorimeters the dependence of e/h on material thicknesses is understood as follows.

– The electron sampling fraction e is approximately proportional to the ratio of scintillator thickness d_{sc} to absorber thickness d_U.

– For the hadron sampling fraction h, the energy from the electromagnetic component and the ionization loss from directly produced charged particles is again proportional to d_{sc}/d_U. The nuclear binding energy is not detected whereas the energy detected from low energy neutrons is approximately independent of d_{sc}/d_U, the reason being that low energy neutrons are efficiently detected in the plastic scintillator via elastic scattering on protons, but hardly lose energy by elastic collisions in the high A absorber material. The fraction of the energy lost to break up the nuclear binding energy is correlated to the number and energy of the produced neutrons. This fact can be used to achieve an optimum energy resolution if the correlation is preserved in the energy measurement for each event.

The different dependence of e and h on the material thicknesses d_{sc} and d_U allows tuning e/h and the hadronic energy resolution [3]. It has been shown that a ratio $e/h = 1$ can be achieved for approximately equal thickness of uranium and scintillator [2].

Most of the neutrons produced in uranium come

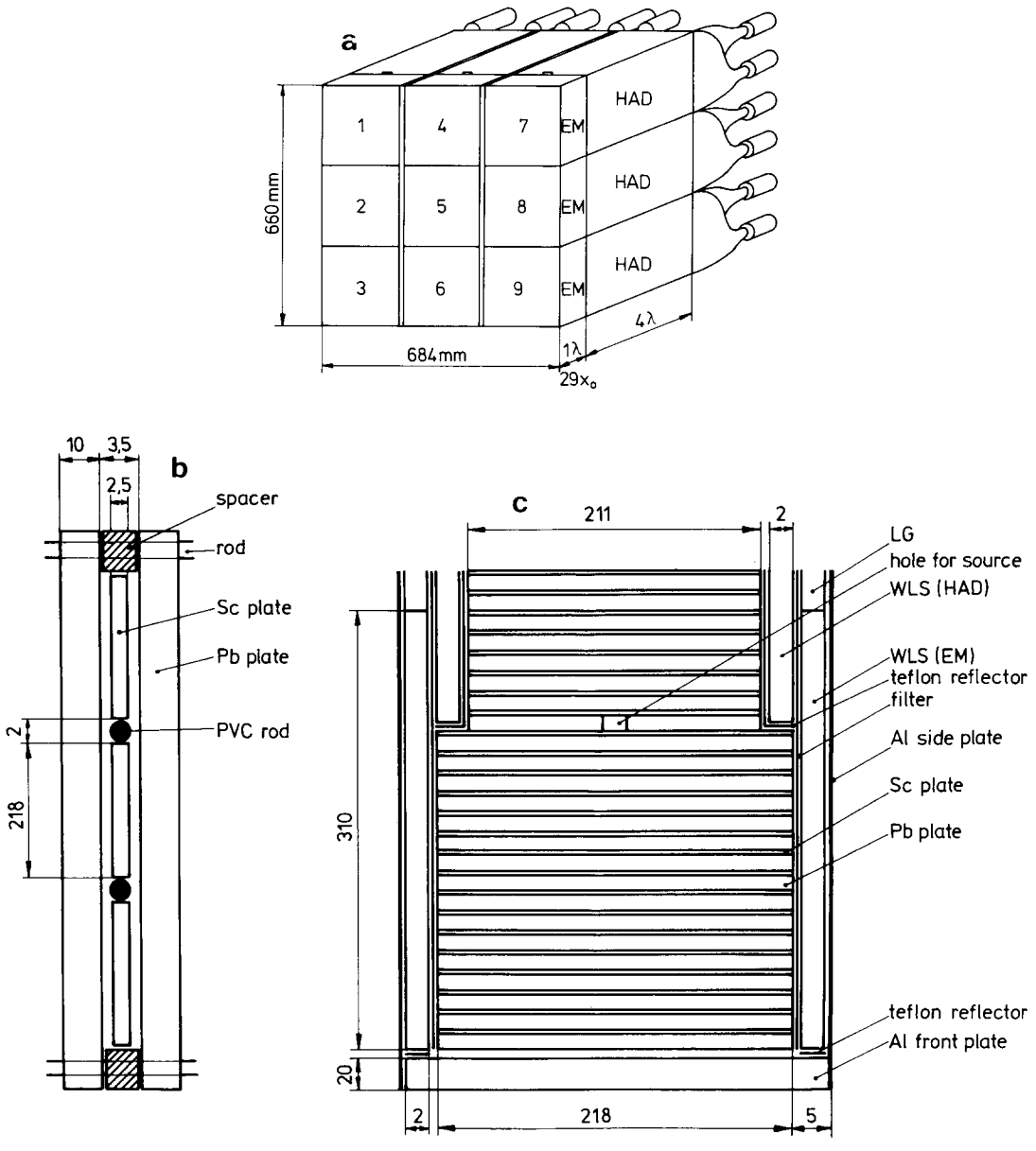

Fig. 1. (a) Schematic view of the calorimeter with details about dimensions, segmentation and tower numbering. There is a separate readout for the electromagnetic section (EM) and for the hadronic section (HAD). (b) Layer structure of one module. All dimensions are in mm. The figure is not drawn to scale. (c) Readout structure of one module as seen from the top. Note the hole in the lead plate number 17 to insert the calibration source.

from evaporation of highly excited nuclei, with smaller contributions from spallation or fission processes. Typical neutron kinetic energies are 2 MeV and typical yields are 33 neutrons below 20 MeV, per GeV of incident hadron energy [4]. If lead instead of uranium is considered as absorber the same processes are present but the neutron yield is only about 22 per GeV, with a similar energy distribution. Following these arguments, it has been proposed that lead–scintillator calorimeters can also be compensating provided that the signal due to slow neutrons compared to the signal of ionizing particles is enhanced by an adequate choice of the sampling ratio [5]. The recommended ratio varies between 3 and 5 [6]. For a typical scintillator thickness of 2.5 mm it requires very thick lead plates of 7.5–12.5 mm. In order to investigate this possibility we have decided to build and test a calorimeter with a lead to scintillator ratio of 4 to 1.

2. Description of the calorimeter

The calorimeter consisted of three identical modules (see fig. 1a). Each module was subdivided vertically into three optically decoupled towers. The front part of each tower (EM section) and the back part (HAD section) had separate readout. The depth of the EM section was $29X_0$ (radiation length) or 1λ (hadronic interaction length). The HAD section was 4λ deep. In this way, a calorimeter of nine towers with a total depth of 5λ for hadronic interactions was built.

Each module had a sandwich structure of 81 layers. The sampling layer (see fig. 1b) consisted of a 10 mm thick lead plate followed by a 2.5 mm thick scintillator sheet. The lead plates contained 4% antimony to increase the mechanical stability. They were kept at a distance by 3.5 mm thick spacers located at the top and bottom of the plate. The stack was held together by high quality steel rods running through the spacers. In this way no dead material was introduced in the sensitive volume. The dimensions of the lead plates were 70×21.8 cm^2 in the EM section and 70×21.1 cm^2 in the HAD section. The dimensions of the scintillator sheets were 21.8×21.8 cm^2 and 21.8×21.1 cm^2 respectively. They were polished on all sides and wrapped in white paper except at the readout edges. The scintillator material used was SCSN-38 [7]. The three scintillator sheets in each layer were separated by 2 mm thick PVC rods. The EM section contained the first 16 layers and the HAD part the remaining 65 layers.

Each tower was read out on both sides (see fig. 1c) by 2 mm thick wavelength shifter plates (WLS). The light collected by these plates was transmitted to photomultipliers (PM) of the type XP2011 from Philips, via plexiglass light guides (LG). The WLS plates consisted of a PMMA base UV absorbant, doped with K27 [8] in a concentration of 125 mg/l. The length of these plates was 31.0 cm for the EM section and 91.8 cm for the HAD section. They were covered on the face opposite to the scintillator plates by reflective aluminum foil. In order to achieve a good uniformity in light collection, a graded grey filter compensating for the light attenuation along the WLS was inserted in between the WLS plate and the scintillator. In addition a teflon reflector covered the edge opposite to the photomultiplier. Details of the calorimeter modules are summarized in table 1.

Table 1
Calorimeter module parameters

	EM section	HAD section
Number of Pb plates	16	65
Number of sc plates	16	65
Size of Pb plates (mm^3)	$700\times218\times10$	$700\times211\times10$
Size of sc plates (mm^3)	$218\times218\times2.5$	$211\times218\times2.5$
Size of WLS plates (mm^3)	$218\times310\times2.0$	$218\times918\times2.0$
Optical channels per module	6	6
Material Pb plates	96%Pb + 4%Sb	
Material sc plates	SCSN-38	
Material WLS plates	PMMA UV-absorbant	
Doping WLS plates	125 mg/l of K27	
Photomultipliers	Philips XP-2011	

3. Experimental setup

For energies below 10 GeV the calorimeter was exposed to the T7 beam of the CERN PS. This beam provided electrons, muons and hadrons (essentially pions if the negative charge is selected) up to an energy of 10 GeV. We estimate the momentum spread of this beam to be less than 2% for the collimator settings used during the measurements. The modules were installed on a moving support allowing a horizontal scan of the central towers (2, 5 and 8).

The beam was defined by four scintillation trigger counters: B1, B2, B3 and B4 (see fig. 2a). B3 was a narrow finger counter used to define precisely the beam spot, and B4, with a 1 cm diameter hole in the middle, was used as veto counter to reject beam halo events. An additional counter B5 was located behind the calorimeter and was used to tag muons. Particle identification was provided by two Cherenkov counters, C1 and C2, filled with CO_2 gas. Their pressure was adjusted above the muon threshold to optimize the electron recognition.

The Cherenkov counter C2 and the five scintillation counters were used to define three different trigger conditions (see fig. 2a). The beam condition was a coincidence between B1, B2, B3 and no veto given by B4. The electron trigger required in addition a signal in C2. The muon trigger required a signal in B5 in coincidence with the beam, but excluding B3 in order to increase the event rate. The hadron trigger corresponded to the beam condition. The hadron content of this beam was about 60% at 3 GeV increasing up to 90% at 10 GeV. The muon content was about 3% at all energies, the rest being electrons.

For each event accepted by the trigger, the photomultiplier signals were integrated by a LeCroy 2282B ADC unit of 12 bits with a gate time of 150 ns. The output of this unit was read out by a computer based on a Motorola 68020 processor and transferred to magnetic tape for offline analysis.

All the measurements were performed with negative charged particles.

For data taking at higher energies (10–75 GeV) the calorimeter was moved to the X5 beam of the CERN SPS. The experimental setup (see fig. 2b) was very similar to the one used at the PS with the following modifications:

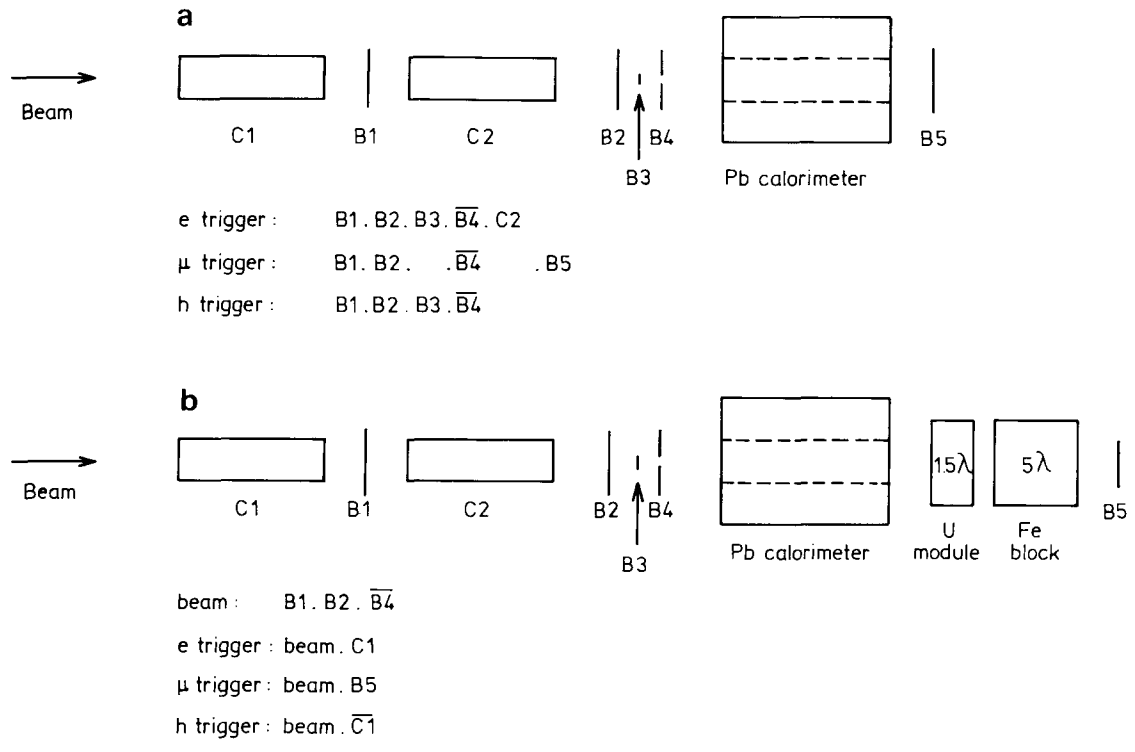

Fig. 2. (a) Experimental layout and trigger conditions at the PS. (b) Experimental layout and trigger conditions at the SPS.

– The calorimeter was installed on a support allowing both the horizontal and the vertical movement so the centre of all nine towers could be reached by the beam.

– A uranium–scintillator module 1.5λ deep was placed as tail catcher about 80 cm behind the lead calorimeter. A calorimeter consisting of four of these modules showed in a previous test an energy resolution of about $35\%/\sqrt{E}$ and almost equal response for electrons and hadrons [9]. The calibration of this uranium module was obtained with electrons. An iron absorber 5λ deep was also installed between this uranium module and the muon tagger.

– The Cherenkov counters were filled with helium and nitrogen respectively. Their pressures were adjusted in the same way as at the PS. In order to increase the event rate, the counter B3 was removed from the trigger. The beam spot was then defined by a 2 cm diameter hole in B4.

– The hadron trigger condition included also one Cherenkov counter as veto against electrons. The resulting particle content of this trigger condition was 60% hadrons at 10 GeV, increasing up to 85% at 75 GeV. The muon content was about 5% in the whole energy range, the rest being electrons.

– The signals from the calorimeter were split passively at the photomultiplier into a $\frac{3}{4}$ and a $\frac{1}{4}$ fraction. The signal cable between the split and the ADC was long enough to avoid the influence of reflections. In this way the muon signal appeared well separated from the pedestal of the ADC and at the same time the saturation of the ADC at the highest energies was avoided for the $\frac{1}{4}$ fraction of the signal.

– The computer used for the data acquisition was a PDP-11.

4. Event selection

The criteria used to isolate samples of electrons, muons and hadrons in the offline analysis were based on the signals delivered by the Cherenkov counters, the muon tagger and the calorimeter itself.

In fig. 3 we plot the quantity $C_{12} = C_1 + C_2$, where C_1 and C_2 are the signals of the Cherenkov counters, for beam energies of 5, 10 and 50 GeV respectively. This quantity helps to separate electrons from hadrons especially at low energies. Electrons were selected by a cut on C_{12} and by requiring that the total energy deposited outside the electromagnetic section of the central tower, on which the beam is incident, is smaller than 500 MeV. In this way the residual contamination of hadrons and pileup events was removed. We estimate the contamination of this electron sample to be around 0.1%.

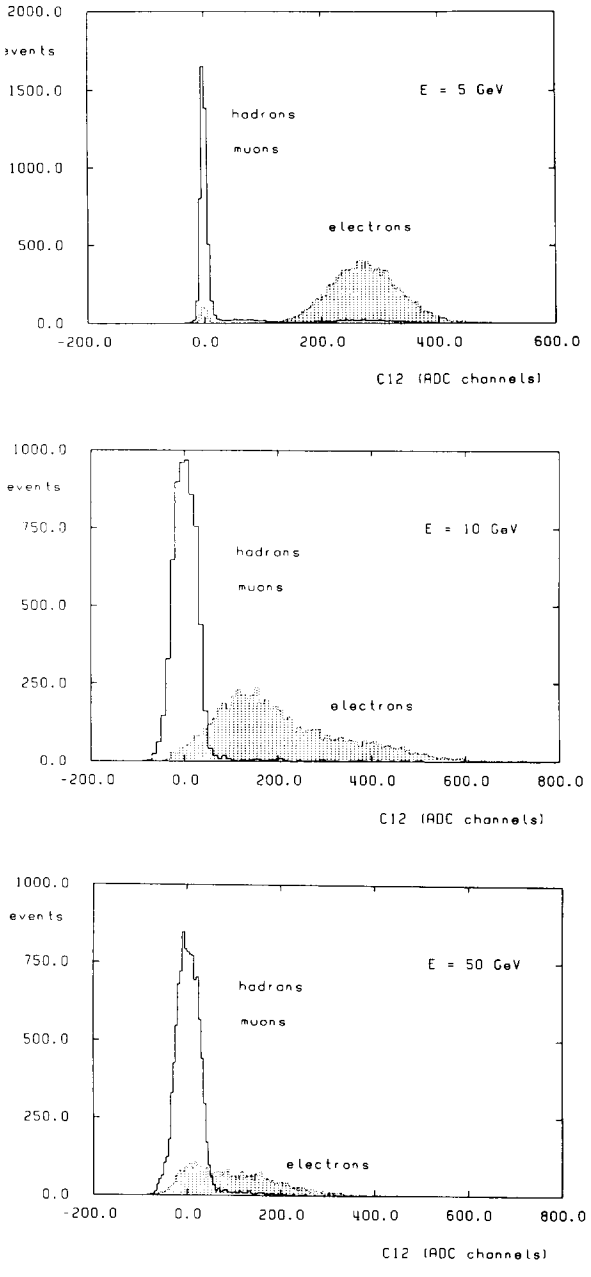

Fig. 3. Sum of the two Cherenkov signals for beam energies of 5, 10 and 50 GeV and for all events. The 5 GeV data correspond to the PS setup and the others to the SPS setup. Electrons and hadrons are selected by imposing cuts on the calorimeter signals.

For the hadron selection, the energy E_{out} deposited in the outer towers of the calorimeter (all except the central one) was used in addition to the quantity C_{12} previously defined. In fig. 4 we plot for all beam events E_{out} versus the total energy deposited in the calorimeter for energies of 5, 10 and 50 GeV. We observe that electrons, hadrons and muons become well separated in this plot as the energy increases. In order to further suppress the muon contamination inside the hadron sample, all events with a signal in the muon tagger were rejected, but this muon tagger was not fully efficient for geometrical reasons. In order to reject events with energy leakage, additional cuts were applied. They will be

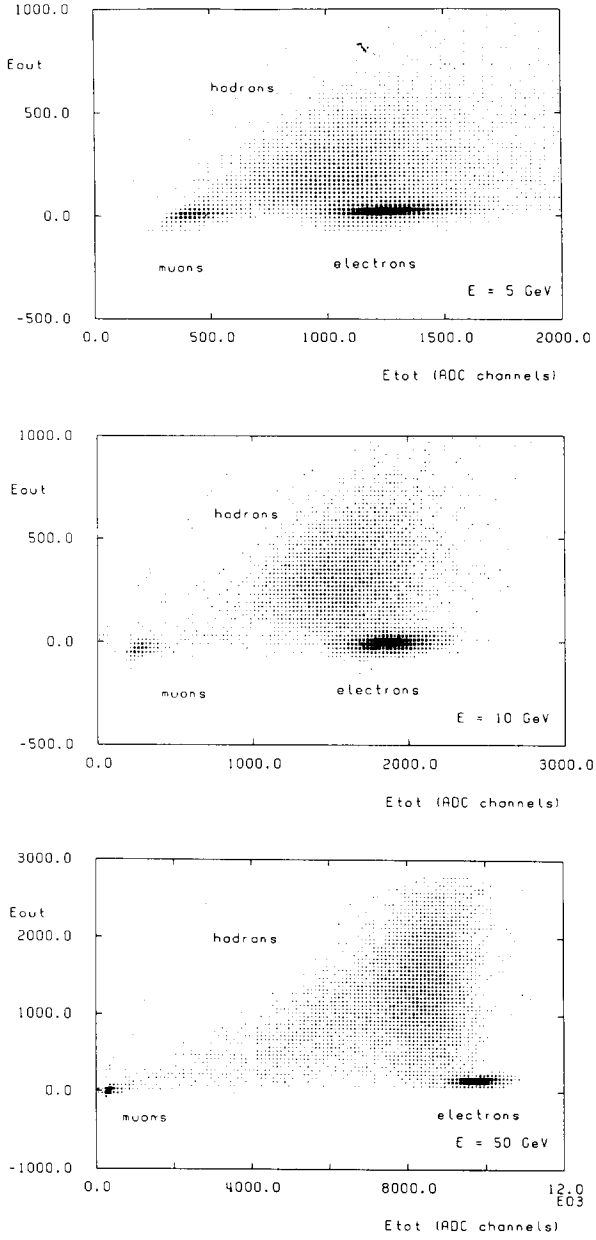

Fig. 4. The energy in the outer towers (E_{out}) versus the total energy (E_{tot}) for all events and beam energies of 5 GeV (PS) and 10 and 50 GeV (SPS). PS and SPS data have different scales.

discussed in detail later. We estimate the contamination of this hadron sample by electrons and muons to be smaller than 1%, and by pileup events at the 2% level below 10 GeV (at the PS). Above 10 GeV (at the SPS) the number of pileup events is negligible since the event rate was much lower.

Muons were selected by requiring a hit in the muon tagger already at the trigger level. In addition only events with a deposited energy in the outer towers smaller than 100 MeV and a good matching between the right and left phototubes of the central tower were accepted. A cut in the total energy was also applied to suppress some residual hadron background.

5. Calibration

For monitoring the gain stability and online calibration of the calorimeter, a ^{60}Co radioactive source of 3 mCi was inserted into a hole in the centre of the lead plate number 17 of each module, which separates the EM and the HAD sections (see fig. 1c). The HV of all phototubes were adjusted with the help of this source using a 10 μs gating time for the ADC. These measurements were performed in regular intervals during running in order to check the gain stability of the photomultipliers. This was the only way to calibrate the whole detector at the PS since the beam could only reach the centres of three of the nine towers. The ^{60}Co source calibration was compared for these three towers to a calibration with electrons, hadrons and muons, showing differences of 5%. The reason for these differences is that the source irradiates only the closest scintillator plates, whereas all plates contribute to the signal for beam particles.

At the SPS all nine towers could be calibrated with the beam and therefore the source method was only used for a first online calibration. For the offline analysis, all the phototube signals of the EM section were equalized for 10 GeV electrons and all phototubes of the HAD section for 10 GeV hadrons. In the EM section the difference between the electron and the hadron calibration was $\pm 1\%$ and the difference between the electron and the muon calibration was $\pm 5\%$. In the HAD section the difference between the hadron and the muon calibration was $\pm 2\%$.

The relative calibration between the EM and the HAD sections was obtained by multiplying the gain of all HAD sections by a factor α and demanding that the fractional energy resolution for hadrons, σ_E/E, is minimal. In fig. 5a we plot this energy resolution as a function of α for 10 and 50 GeV. Another method based on the ratio between the muon signal in the two sections gave compatible results within errors. In first approximation this ratio should be equal to the ratio of the number of plates, $65/16 = 4.06$, but it is modified

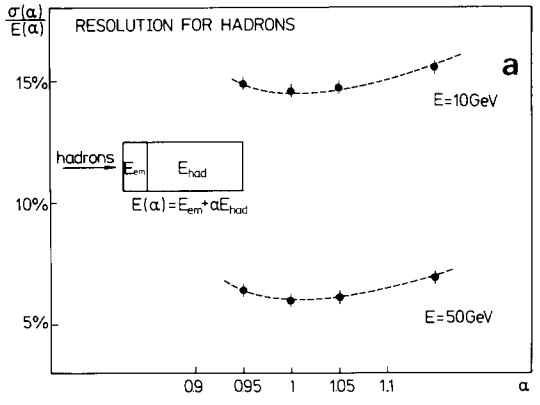

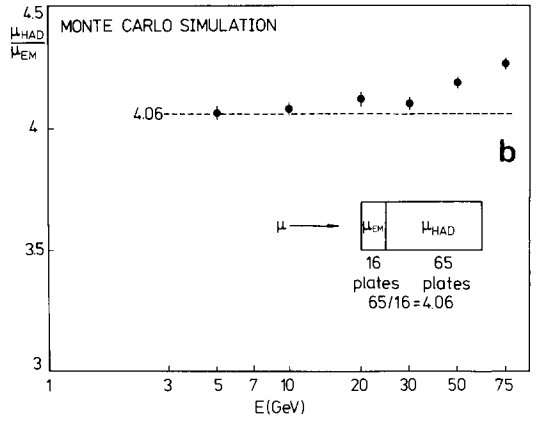

Fig. 5. (a) Energy resolution for hadrons as a function of the global calibration of the HAD section α for beam energies of 10 and 50 GeV. (b) Monte Carlo prediction for the ratio between the mean muon signal in the HAD and in the EM sections as a function of the beam energy in logarithmic scale.

by radiation effects, especially at high energies, as shown by some Monte Carlo calculations using the GEANT3 event generator [10] (see fig. 5b). This correction had to be taken into account in our case since 50 GeV muons were used for calibration; it amounted to about 5%.

6. Uniformity

In order to determine the transverse uniformity of light collection, we performed a horizontal and a vertical scan of the central tower with electrons. The uniformity of light collection along the WLS was also checked by bench test measurements prior to the construction of the modules and using a ^{60}Co source for the assembled modules.

The horizontal scan was performed at the PS with 5 GeV electrons in steps of 2 cm. The result is displayed in fig. 6a. The response is seen to be uniform within

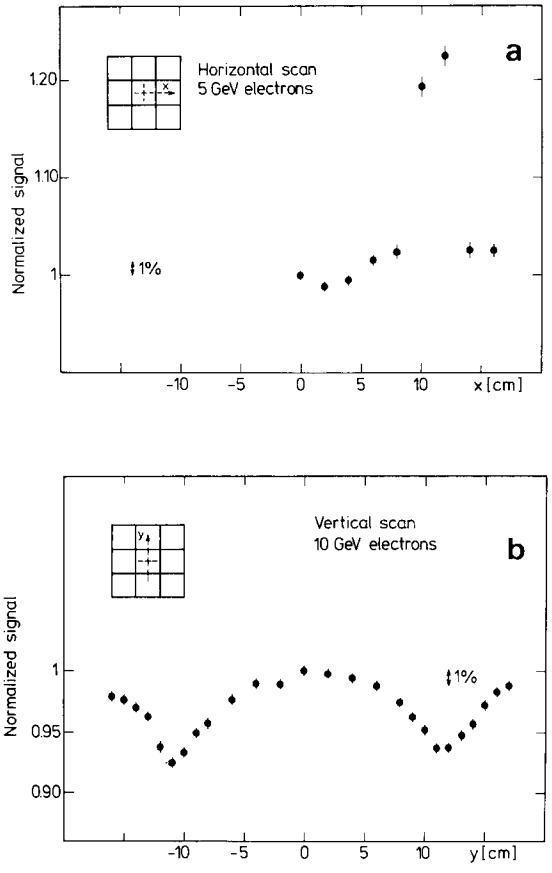

Fig. 6. (a) Result of a horizontal scan of the central tower with 5 GeV electrons. The signal is normalized to the value at the centre of tower 5. (b) Result of a vertical scan of the central tower with 10 GeV electrons. The signal is normalized to the value at the centre of tower 5.

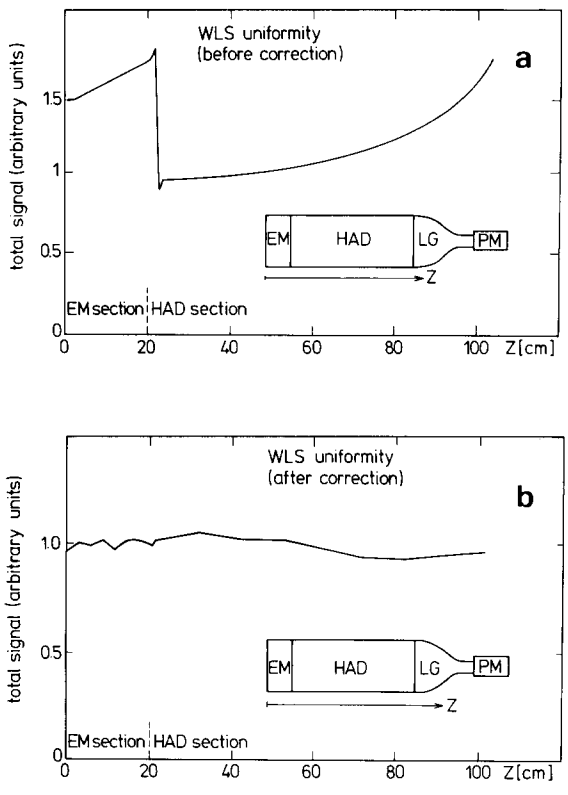

Fig. 7. (a) Result of a bench test measurement of the WLS uniformity without any correction. (b) Result of a bench test measurement of the WLS uniformity after insertion of a front reflector and dotted filters.

$\pm 1\%$ in a region of ± 6 cm around the centre of the tower. At the edge of the plate we observe an enhancement of about 20%. This effect can be attributed to an increase in light yield at the edge of the scintillator plate and to light produced in the WLS itself. The effective attenuation length of light inside the scintillator plate was found to be about 60 cm.

The vertical scan was performed at the SPS with 10 GeV electrons in steps of 1 cm. The response was again found to be uniform within $\pm 1\%$ in a region of ± 6 cm around the centre of the scintillator plate (see fig. 6b). The drop of 8% at the edge of the plate can be attributed to a decrease in light yield in a region close to a reflecting surface, and to the dead area introduced by the PVC rods.

The uniformity of light collection along the WLS was optimized in bench test measurements. The length of the WLS plate was about 10 cm longer than geometrically required for the EM section (see fig. 1c) in order to reduce the sharp increase in light yield towards the readout side. This correction, however, was insufficient to achieve the required uniformity as seen in fig. 7a. The HAD part showed at the same time a difference in light yield between both ends of 80%. These nonuniformities were suppressed by inserting transparent foils with dots of varying density between the WLS and the scintillator, and a teflon front reflector as mentioned in section 2 (see again fig. 1c). After these corrections the nonuniformities were reduced to $\pm 5\%$ (see fig. 7b).

7. Electron signal and light yield

We measured the response of the calorimeter to electrons incident at the centre of tower 5. Each EM section is $29X_0$ deep and 22 cm wide (to be compared with a Molière radius of about 2.5 cm) and therefore contains fully electron showers at all energies.

For each energy we fitted a Gaussian to the pulse height distribution, obtaining in such a way the mean value $\langle E_e \rangle$ and the energy resolution σ_e. In fig. 8 the pulse height distributions for beam energies of 5, 10 and 50 GeV are plotted with the corresponding fits.

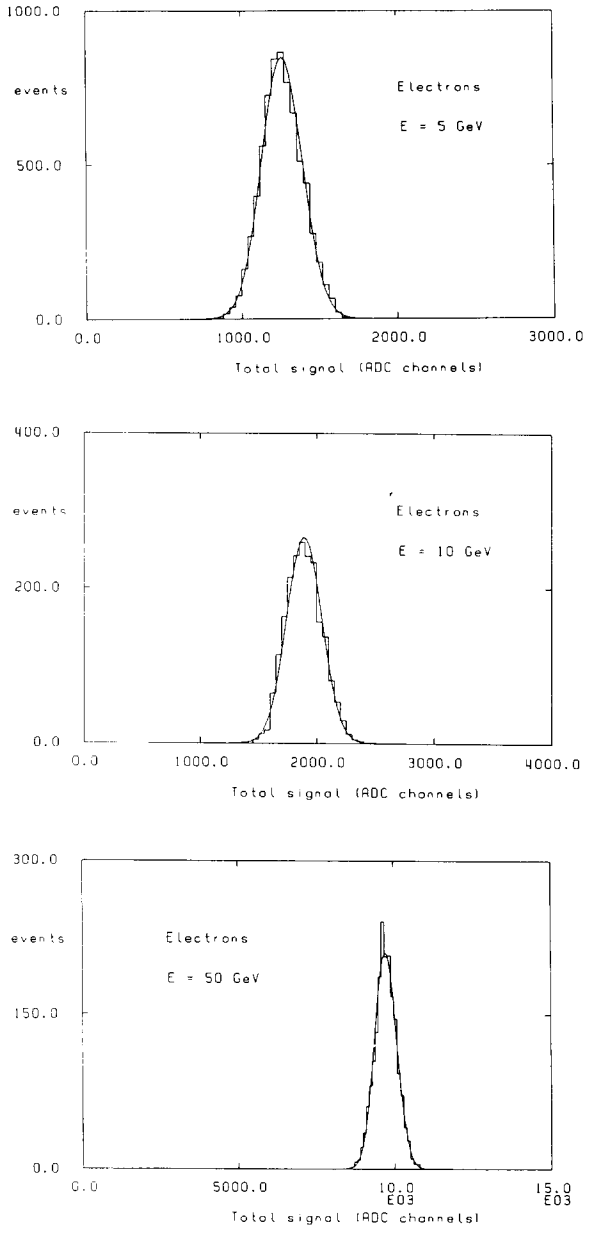

Fig. 8. Electron signal for 5 GeV (PS) and 10 and 50 GeV (SPS) beam energies. PS and SPS data have different scales.

The deviation from linearity of the mean electron response as a function of the beam energy can be deduced from fig. 9a. It shows δ, the mean response divided by the beam energy and normalized to one when averaged over all energies. The normalisation is different for PS and SPS data due to differences in the gain of the phototubes. We conclude that the calorimeter response to electrons is linear within 1%.

Fig. 9b displays the energy resolution: $[\sigma_e/\langle E_e\rangle]\sqrt{E}$. Apart from a small increase at high energies compatible with the beam momentum spread, this quantity is constant as expected for a calorimeter where the energy resolution is dominated by sampling fluctuations. The following parametrization:

$$\frac{\sigma_e}{\langle E_e\rangle} = \frac{a}{\sqrt{E}} \oplus b \qquad (E \text{ in GeV}),$$

where $\oplus$ means a quadratic sum, leads to:

$$a = (23.5 \pm 0.2)\% \qquad \text{and} \qquad b = (1.2 \pm 0.2)\%.$$

The $\sqrt{E}$ dependent term contains the contribution from sampling fluctuations and from photoelectron statistics. The latter was determined from the width σ_d of the distribution $R-L$ where R and L are respectively the pulse heights of the left and right phototubes. This quantity σ_d is also plotted in fig. 9b. We obtain:

$$\frac{\sigma_d}{\langle E_e\rangle} = \frac{(6.6 \pm 0.1)\%}{\sqrt{E}} \qquad (E \text{ in GeV}).$$

We did not include here the data taken at the SPS since

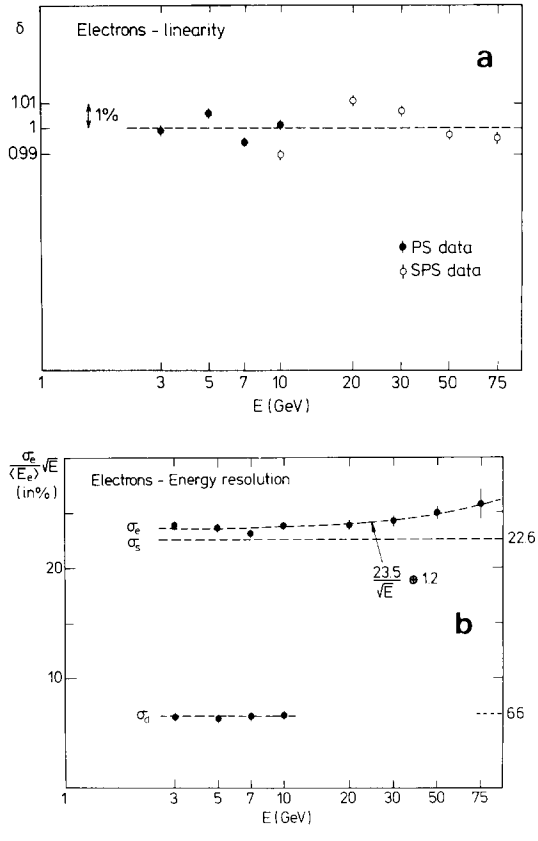

Fig. 9. (a) Linearity of the electron response. The beam energy is in logarithmic scale. PS and SPS data have separate normalisations. (b) Energy resolution for electrons as a function of the beam energy in logarithmic scale. The contribution from sampling fluctuations (σ_s) and from photoelectron statistics (σ_d) are also indicated.

the finger counter B3 was not used and σ_d is sensitive to the beam spot size, especially at high energies.

The contribution from sampling fluctuations alone is:

$$\frac{\sigma_s}{\langle E_e \rangle} = \frac{\sigma_e}{\langle E_e \rangle} \ominus \frac{\sigma_d}{\langle E_e \rangle} = \frac{(22.6 \pm 0.2)\%}{\sqrt{E}},$$

where $\ominus$ means a quadratic subtraction.

The EGS4 Monte Carlo generator [11] predicts an energy resolution of $\sigma_s/\langle E_e \rangle = (22.0 \pm 0.5)\%/\sqrt{E}$ compatible with our measurement. We observe that the energy resolution is only slightly affected by the photoelectron statistics.

Assuming approximately equal light transmission and quantum efficiencies for the left and right phototubes, the light yield can be determined in the following way:

$$N_{pe} = \left[\frac{\sigma_d}{\langle E_e \rangle}\right]^{-2},$$

with N_{pe} being the number of photoelectrons measured for a shower of energy E, summing both PMs. We find $N_{pe} = 230$ per GeV of incoming energy. The Monte Carlo prediction for the fraction of incident energy deposited in the scintillator is 2.4%. Thus we measure in the EM section of the calorimeter 9.6 photoelectrons per MeV of deposited energy in the scintillator.

8. Hadron signal and the e/h ratio

We measured the response to hadrons incident at the centre of tower 5. The visible energy in different sections of the calorimeter is plotted in fig. 10a. We observe that the energy contained in tower 5 (E_{in}) is equal to about 80% of the total signal at all energies. The energy contained in the EM section (E_{em}) decreases from 50% at 3 GeV to 30% at the highest energies. We therefore expect a side leakage rather energy independent and a back leakage increasing with energy. The average side leakage was determined from the energy deposition in the individual modules when the beam is incident at the centre of the outer towers. To estimate the average back leakage we used the energy deposited in the uranium module located behind the lead calorimeter as described in section 3. These measurements are plotted in fig. 10b. We observe a 4–5% average side leakage and an average back leakage negligible below 10 GeV and increasing up to 8% at 75 GeV. We note that the uranium module was too far away from the lead calorimeter to contain all the back leakage.

The distribution of the side and back leakage are markedly different. Fig. 11a shows the signal summed over the outer towers (3, 6, 7, 8 and 9) for 10 GeV hadrons incident at the centre of tower 1. This signal

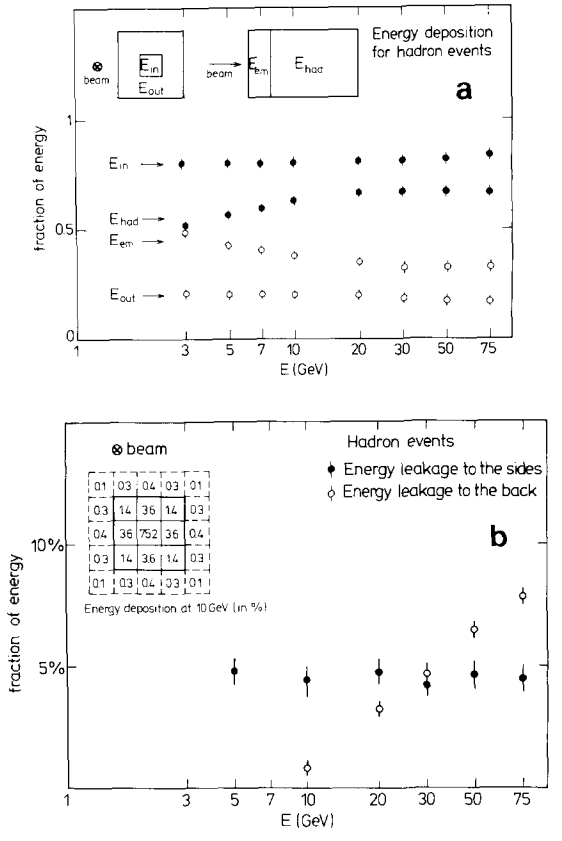

Fig. 10. (a) Hadron deposition in different sections of the calorimeter as a function of the beam energy in logarithmic scale. E_{in} is the energy deposited in the inner tower, E_{out} in the outer towers, E_{em} in the EM sections and E_{had} in the HAD sections. (b) An estimation of the energy leakage for hadrons showers at different energies. The energies depositon in the different towers at 10 GeV is also displayed.

represents about 30% of the total side leakage when the beam is incident at the centre of tower 5. The width of this distribution is small compared to the width of the total energy distribution. Fig. 11b shows the signal in the uranium module for 50 GeV hadrons. We observe again a narrow distribution peaked at zero, but in addition a long tail. The effect of longitudinal leakage on the energy contained in the lead calorimeter at high energies will then be a small shift in the peak of the distribution (similar to the side leakage) and a long tail towards lower measured energies. This indicates that a 5λ calorimeter is too short for full containment at high energies. As a consequence, the energy resolution can only be determined after removing events with a significant back leakage. Since this can introduce a bias in the results we have used two different selection methods for a cross-check:

Method 1: All events with a deposited energy in the uranium module greater than 1 GeV were rejected. This

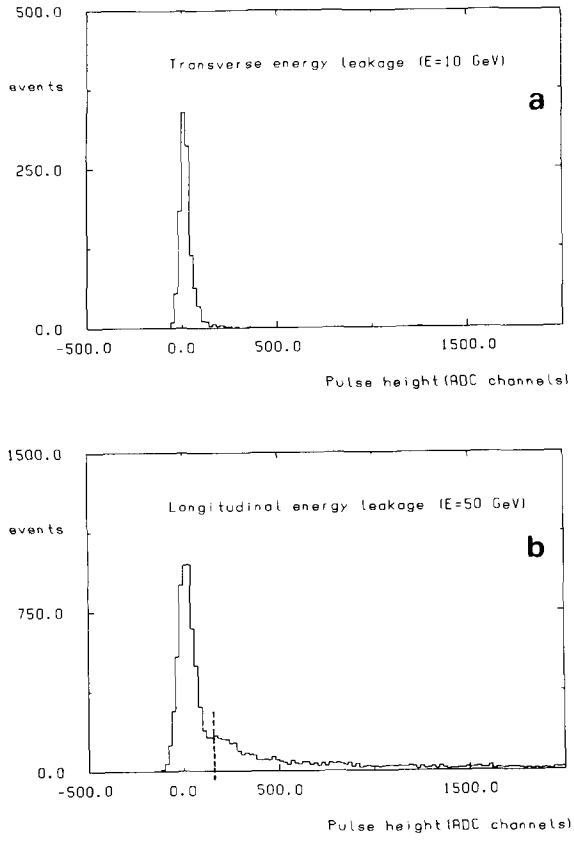

Fig. 11. (a) Signal in towers 3, 6, 7, 8 and 9 for 10 GeV hadrons incident at the centre of tower 1. This signal corresponds to about 30% of the side leakage for a beam incident at the centre of the calorimeter. (b) Signal in the uranium module for 50 GeV hadrons. This signal is an estimation of the back leakage. The position of the cut used to select events according to method 1 is indicated.

cut reduced the hadron sample by only 3% at 10 GeV, but at 75 GeV the rejection was as big as 50% (see fig. 14a). The rejected events are mainly late showering events or events with a big shower length.

Method 2: All events with a deposited energy in the EM section of the calorimeter smaller than 1.5 GeV were rejected. The EM signal distributions for energies of 10 and 50 GeV are plotted in fig. 12. We observe that the rejected events behave in the EM section as minimum ionizing particles. This cut essentially forces the shower to start in the first λ of the calorimeter. The energy deposited in the uranium module was then simply added to the energy deposited in the lead calorimeter. In this way about 55% of the hadronic events were selected, rather independent of the beam energy (see fig. 14a).

For each energy and for both hadron samples we fitted Gaussians to the pulse height distributions, obtaining the mean value $\langle E_h \rangle$ and the resolution σ_h. Data and fits are shown in fig. 13 for 5, 10 and 50 GeV (for events selected according to method 1). The distributions exhibit small tails. The effect of these tails on the energy resolution has been suppressed by fitting exclusively the region inside two standard deviations around the mean value, as shown in the figures.

The measured ratio between the mean value $\langle E_e \rangle$ for electrons and the mean value $\langle E_h \rangle$ for hadrons is displayed as a function of the beam energy in fig. 14b. Methods 1 and 2 give identical results. This ratio varies from 1.19 a 3 GeV to 1.09 at 75 GeV. For energies above 10 GeV, it is consistent with a constant value of 1.10. This measurement can be affected by many instrumental effects: calibration errors (since many towers are involved), energy leakage, dead areas inside the calorimeter, nonuniformities in light collection and finally event contamination and pileup. Some of these effects certainly contribute to the observed tails in the pulse height distributions. The photoelectron statistics and the beam momentum spread produce negligible effects. We have not tried to correct our e/h measurement for

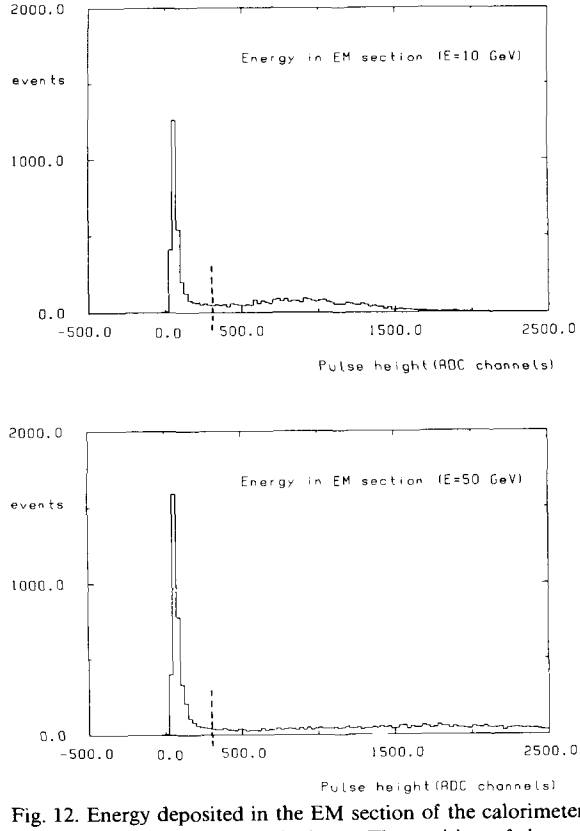

Fig. 12. Energy deposited in the EM section of the calorimeter for 10 and 50 GeV incident hadrons. The position of the cut used to select events according to method 2 is indicated.

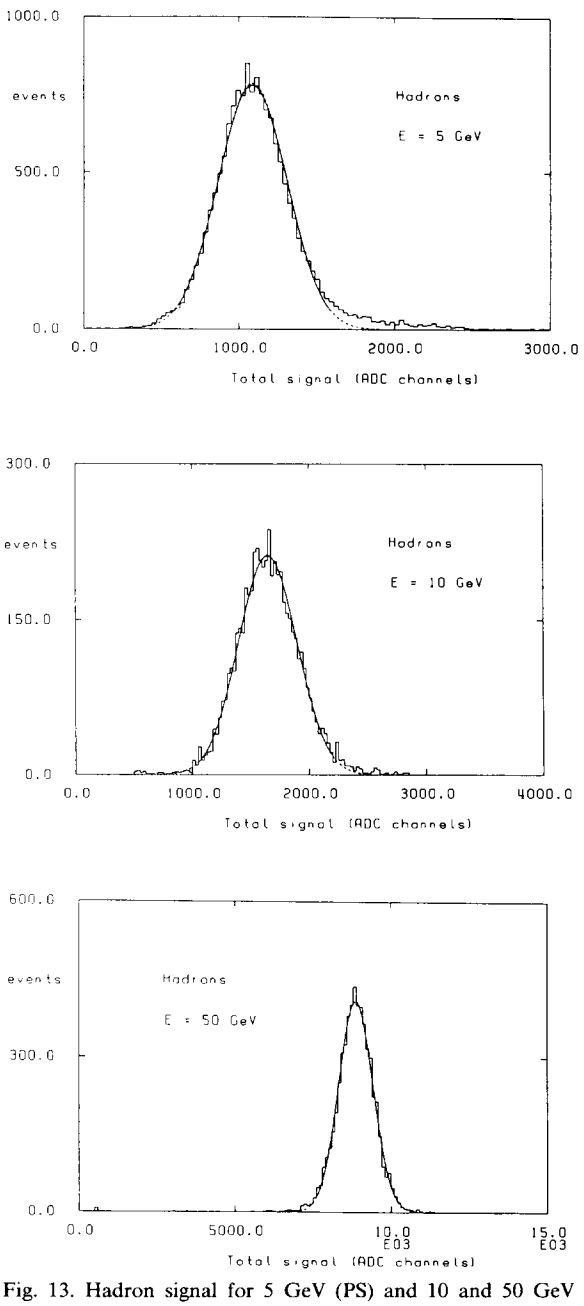

Fig. 13. Hadron signal for 5 GeV (PS) and 10 and 50 GeV (SPS) beam energies. The tail at 5 GeV is due to pileup events. PS and SPS data have different scales.

any of the previously mentioned effects, that we believe small, except for the observed energy leakage to the sides of about 5%. We have estimated the effect of the calibration error to be about 3% and the total error about 4%. Therefore:

$$\frac{e}{h} = 1.05 \pm 0.04 \qquad \text{for} \quad E > 10 \text{ GeV}.$$

We conclude that the thickness ratio of 4 to 1 between lead and scintillator is not far from providing exact compensation. In fact our analysis does not exclude that this compensation has already been reached.

The energy resolution σ_h is displayed as a function of the beam energy in fig. 15a (method 1) and fig. 15b (method 2). Up to 50 GeV both methods give compatible results. The fractional energy resolution is proportional to $1/\sqrt{E}$ as for electrons. At 75 GeV the resolution obtained by method 2 is worse by 10%. We attribute this effect to an incomplete containment of showers in the uranium module. The pulse height distributions for 75 GeV hadrons selected by method 1 and 2 are shown in fig. 16a and 16b respectively. The systematic error due to calibration and other effects has been estimated to be about 3%. We find therefore an average energy resolution of:

$$\frac{\sigma_h}{\langle E_h \rangle} = \frac{(44.2 \pm 1.3)\%}{\sqrt{E}}.$$

This result has been obtained from the hadron sample

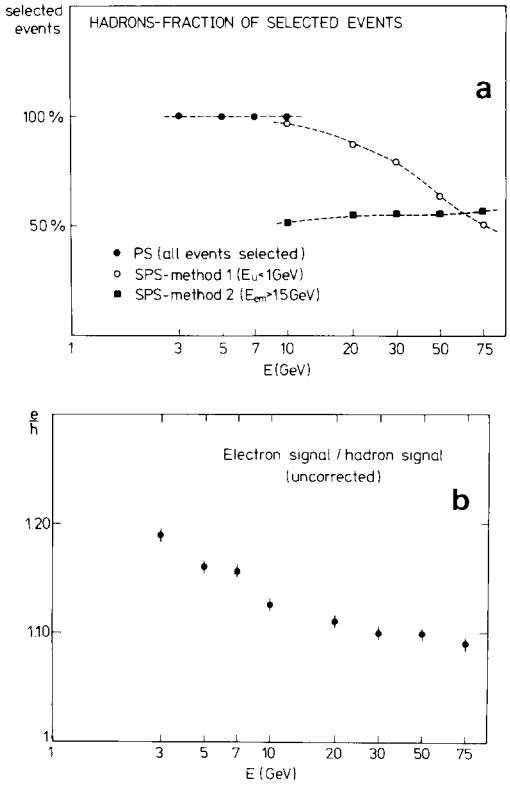

Fig. 14. (a) Fraction of hadronic events selected from the total sample according to method 1 ($E_U < 1$ GeV) and method 2 ($E_{em} > 1.5$ GeV). The dotted lines are drawn only to guide the eye. (b) The uncorrected e/h ratio as a function of the beam energy. The energy scale is logarithmic.

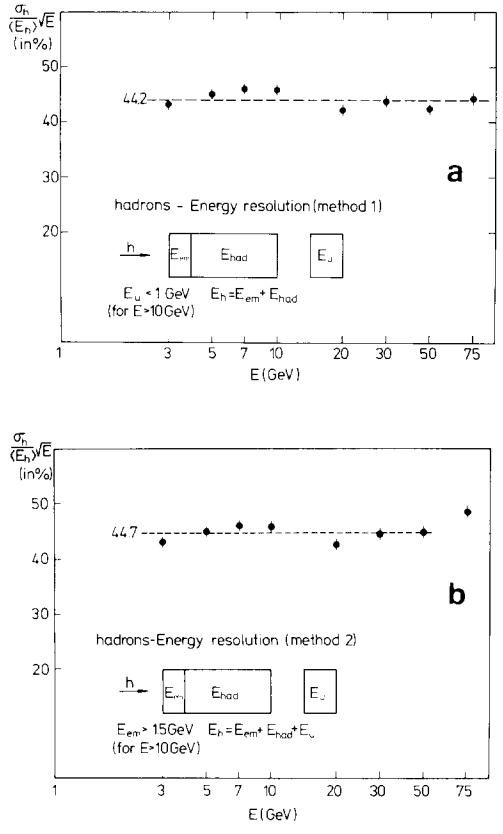

Fig. 15. (a) Energy resolution for hadrons versus beam energy in logarithmic scale. The events are selected by requiring $E_u < 1$ GeV (method 1). (b) Energy resolution for hadrons versus beam energy in logarithmic scale. The events are selected by requiring $E_{em} > 1.5$ GeV (method 2).

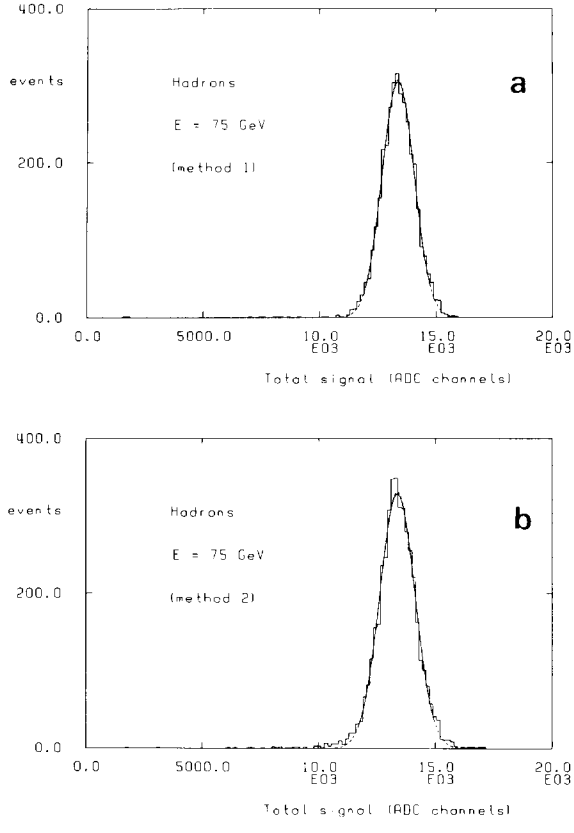

Fig. 16. (a) Hadron signal for 75 GeV beam energy. The events are selected according to method 1. (b) Hadron signal for 75 GeV beam energy. The events are selected according to method 2.

selected according to method 1. As far as we can check, it is representative of all hadronic events.

9. Muon signal and the e/mip ratio

The muon signal was used to obtain a scale in MeV for the energy measured in the scintillator. We followed a method based on the most probable value (mpv) of the muon pulse height distribution. According to the Landau theory [12], the most probable energy deposited in the scintillator is:

$$\Delta_{\mathrm{mpv}}(\mathrm{MeV}) = \Delta_{\mathrm{mean}} + \xi(0.20 + \beta^2 + \ln \kappa)$$

with $\kappa = \xi/\Delta_{\max}$, where Δ_{mean} is the mean energy given by the Bethe–Bloch formula, $\Delta_{\max}$ is the maximum energy transferred in a single collision and β is the speed of the muon. The quantity ξ is proportional to the thickness of scintillator traversed by the muon. For the 16 scintillator sheets of the EM section we obtain $\xi = 0.350$ MeV. The constants necessary to calculate Δ_{mean} and ξ have been taken from ref. [13]. The parameter κ is smaller than 10^{-3} in our energy range and therefore the Landau theory is applicable. We have neglected that energy can be transferred from the absorber to the scintillator and vice versa.

The value of Δ_{mpv} in ADC channels was obtained by fitting the Moyal function to the observed muon pulse height distributions. The Moyal function [14] is defined as:

$$\Phi(\Delta) = a\ \mathrm{e}^{-\frac{1}{2}(\lambda + \mathrm{e}^{-\lambda})}$$

with

$$\lambda = \left[\Delta - \Delta_{\mathrm{mpv}}(\mathrm{ADC})\right]/b,$$

where a, b and Δ_{mpv} are free parameters. The result of the fit for beam energies of 5, 10 and 50 GeV is shown in fig. 17. The relation between the energy scale in ADC channels and the energy scale in MeV is given by:

$$r = \frac{\Delta_{\mathrm{mpv}}(\mathrm{ADC})}{\Delta_{\mathrm{mpv}}(\mathrm{MeV})}.$$

The ratio between the average energy deposited by

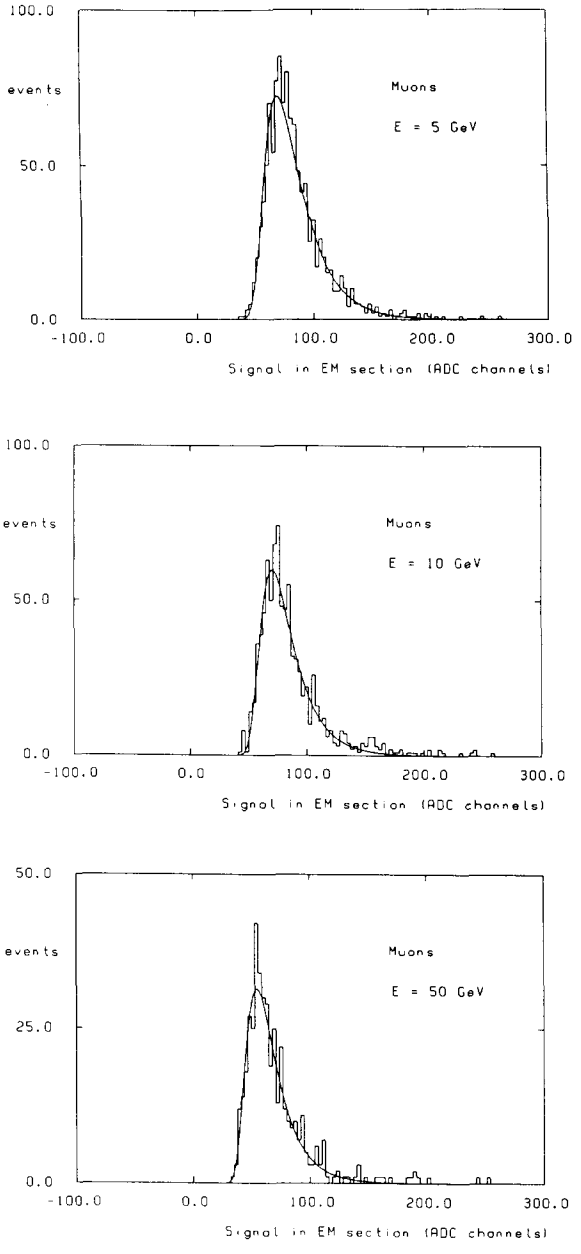

Fig. 17. Muon signal at 5 GeV (PS) and 10 and 50 GeV (SPS) beam energies. PS and SPS data have different scales.

muons in the EM section of the calorimeter and the energy deposited by a minimum ionizing particle (mip) is:

$$\frac{\Delta_\mu}{\Delta_{\mathrm{mip}}} = \frac{1}{r}\frac{\langle E_\mu \rangle}{\Delta_{\mathrm{mip}}},$$

where $\langle E_\mu \rangle$ is the measured mean value of the muon pulse height distribution in ADC channels. According to ref. [15], a mip deposits 2.01 MeV/cm in polystyrene, therefore $\Delta_{\mathrm{mip}} = 8.04$ MeV (we note that a mip is only a hypothetical particle). This ratio is displayed as a function of the muon energy in fig. 18. We observe a significant increase of this quantity with energy.

We also used r to determine the electron sampling fraction:

$$e = \frac{1}{r}\frac{\langle E_e \rangle}{E}.$$

This sampling fraction can be compared to the sampling fraction of a mip. According to ref. [15] the sampling fraction of a mip is 3.75%. We have determined the e/mip ratio for each energy point and the result is also displayed in fig. 18. This ratio is found to be energy independent as expected. The average value is:

$$\frac{e}{\mathrm{mip}} = 0.67 \pm 0.03,$$

where a 5% systematic error has been quoted.

This measurement can be compared to a Monte Carlo calculation using the EGS4 code [11]. In order to obtain a precise value of the electron sampling fraction, cutoff energies of 0.7 and 0.01 MeV for secondary electrons and photons respectively were used. The maximum energy loss per step was also optimized according to the prescription given in ref. [11]. The result of this calculation was $e/\mathrm{mip} = 0.65$ in agreement with the measured value.

10. Summary and conclusions

We have measured the response of a lead–scintillator hadronic calorimeter to electrons, hadrons and muons with energies between 3 and 75 GeV. The calorimeter had a sandwich structure of 10 mm thick lead plates and 2.5 mm thick scintillator sheets. The total depth was 5λ for hadronic interactions and the

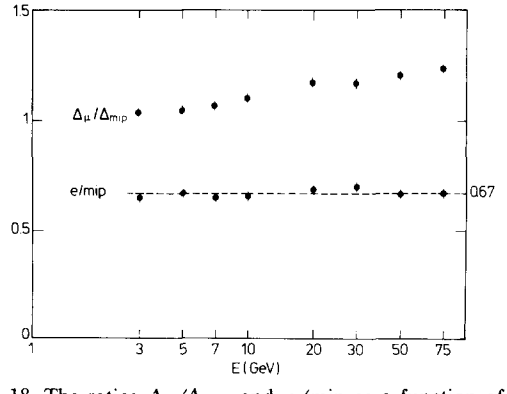

Fig. 18. The ratios $\Delta_\mu/\Delta_{\mathrm{mip}}$ and e/mip as a function of the beam energy. The energy scale is logarithmic.

effective transverse size about 60 cm. The calorimeter was longitudinally segmented in two sections and transversally in nine towers. We have found an energy resolution for electrons of:

$$\frac{\sigma_e}{\langle E_e \rangle} = \frac{(23.5 \pm 0.2)\%}{\sqrt{E}} \qquad (E \text{ in GeV})$$

and an energy resolution for hadrons of:

$$\frac{\sigma_h}{\langle E_h \rangle} = \frac{(44.2 \pm 1.3)\%}{\sqrt{E}} \qquad (E \text{ in GeV}).$$

We have observed for this quantity no departure from a $\sqrt{E}$ dependence up to 50 GeV.

The e/h ratio was found to be almost energy independent for beam energies above 10 GeV. After correcting for an estimated transverse energy leakage of 5%, we have obtained:

$$\frac{e}{h} = 1.05 \pm 0.04 \qquad \text{for} \quad E > 10 \text{ GeV}.$$

We have also estimated an e/mip ratio based on the most probable energy loss of muons in the electromagnetic section of the calorimeter:

$$\frac{e}{\text{mip}} = 0.67 \pm 0.03.$$

If we compare our results with previous measurements with lead–scintillator hadronic calorimeters [16], we conclude that, as theoretically predicted, the increase in the thickness ratio between lead and scintillator has resulted in an equalization of the electron and hadron responses and at the time in a significant improvement in the energy resolution for hadrons.

Acknowledgements

This work has been done in connection with the ZEUS project. We gratefully acknowledge V. Sturm, K. Westphal and W. Zierold as well as R. Pamperin and the DESY workshop for the design and mechanical construction of the modules. We also acknowledge J. Engelen, M. Gallman, A. Legault, J. Lehmann, P. Patel and R. Walzack for help during the data taking at CERN. We would like to thank H. Brückmann and R. Wigmans for helpful discussions, B. Anders and U. Behrens for providing us the Monte Carlo generators and E. Hilger, E. Lohrmann and G. Wolf for encouraging us to perform the experiment. We are grateful for the hospitality extended to us during our stay at CERN and for the support of the CERN-EA division during the setting up and running of the experiment. One of us (M.A.G.) acknowledges CAJAMADRID for financial support.

References

[1] C.W. Fabjan et al., Phys. Lett. 60B (75) 105;
C.W. Fabjan, Calorimetry in High Energy Physics, CERN-EP/85-54, Techniques and Concepts of High Energy Physics III (Plenum, New York, 1985);
J. Bau and T.A. Gabriel, Nucl. Instr. and Meth. A238 (1985) 489.
[2] T. Akesson et al., Nucl. Instr. and Meth. A241 (1985) 17;
B. Anders et al., DESY 86-105; ZEUS collaboration, in preparation.
[3] H. Brückmann, Workshop on Compensated Calorimetry, Pasadena (Sept. 1985).
[4] H. Brückmann, U. Behrens and B. Anders, DESY 86-155;
Experimental measurements of neutron yields can be found in: C. Leroy, Y. Sirois and R. Wigmans, CERN-EP/86-066.
[5] R. Wigmans, CERN-EP/86-141;
B. Anders et al., DPG Frühjahrstagung Teilchenphysik, Zürich (March 1987).
[6] R. Wigmans and H. Brückmann, private communications.
[7] Product of Kyowa Gas, Japan.
[8] Product of Polivar, Italy.
[9] ZEUS collaboration, internal note 87-039 (1987) to be published.
[10] R. Brun et al., CERN DD/EE/84-1 (1986).
[11] W.R. Nelson, H. Hirayama and D.W.O. Rogers, SLAC 265 (1985).
[12] S.M. Seltzer and M.J. Berger, Nat. Ac. of Sciences, Nuclear Science Series 39 (1964).
[13] W. Lohmann, R. Kopp and R. Voss, CERN 85-03 (1985).
[14] J.E. Moyal, Philos. Mag. 46 (1955) 263.
[15] Review of particle properties, Phys. Lett. 170B (1986).
[16] O. Botner, Phys. Scripta 23 (1981) 556;
M.E. Duffy et al., Nucl. Instr. and Meth. 228 (1984) 37.
ZEUS internal note 86-13 (1986) unpublished.